Stochastic Modeling of Flows behind a Square Cylinder with uncertain Reynolds numbers

by

Jacob Kasozi Wamala

Submitted to the
Department of Mechanical Engineering
in Partial Fulfillment of the Requirements for the Degree of

Bachelor of Science in Mechanical Engineering

at the

MASSACHUSETTS INSTITUTE OF TECHNOLOGY

June 2012

Signature of Author _____

Department of Mechanical Engineering
May 16, 2012

Certified by _____

Pierre Lermusiaux
Associate Professor of Mechanical Engineering
Thesis Supervisor

Accepted by _____

John H. Lienhard V
Samuel C. Collins Professor of Mechanical Engineering
Undergraduate Officer

Stochastic Modeling of Flows behind a Square Cylinder with uncertain Reynolds numbers

by

Jacob Kasozi Wamala

Submitted to the Department of Mechanical Engineering
on May 16, 2012 in Partial Fulfillment of the
Requirements for the Degree of

Bachelors of Science in Mechanical Engineering

ABSTRACT

In this thesis, we explore the use of stochastic Navier-Stokes equations through the Dynamically Orthogonal (DO) methodology developed at MIT in the Multidisciplinary Simulation, Estimation, and Assimilation Systems Group. Specifically, we examine the effects of the Reynolds number on stochastic fluid flows behind a square cylinder and evaluate computational schemes to do so. We review existing literature, examine our simulation results and validate the numerical solution. The thesis uses a novel open boundary condition formulation for DO stochastic Navier-Stokes equations, which allows the modeling of a wide range of random inlet boundary conditions with a single DO simulation of low stochastic dimensions, reducing computational costs by orders of magnitude. We first test the numerical convergence and validating the numerics. We then study the sensitivity of the results to several parameters, focusing for the dynamics on the sensitivity to the Reynolds number. For the method, we focus on the sensitivity to the: resolution of in the stochastic subspace, resolution in the physical space and number of open boundary conditions DO modes. Finally, we evaluate and study how key dynamical characteristics of the flow such as the recirculation length and the vortex shedding period vary with the Reynolds number.

Thesis Supervisor: Pierre F. J. Lermusiaux

Title: Associate Professor

Acknowledgements

I would like to extend my gratitude to Professor Pierre Lermusiaux for his assistance during the course of this work, for his helpful direction and for his continued support. I thank Mattheus Ueckermann for his help and mentoring in using the DO/MSEAS code and editing of the document, helpful hints and troubleshooting. Also, for his help this past year as the point person for the MIT Undergraduate Research Opportunities Program (UROP). I am grateful for the help of other graduate students in the MSEAS group in proofreading and discussion contributing to the organization of the thesis. I thank all my friends, especially brothers of Chocolate City at MIT and brothers of the Rho Nu Chapter of Alpha Phi Alpha Fraternity, Incorporated, for their support throughout my undergraduate college years. Most of all, I wish to express my sincerest appreciation to my family, for believing in me and helping me with their support, love, and faith.

Table of Contents

List of Figures

List of Tables

1. Introduction

1.1 Background and Motivation

In recent times, modeling stochastic fluid systems has become increasingly popular as the need and applications for these models has grown while uncertainties in the model parameters, parameterizations and inputs still often remain significant. Stochastic models are applied to varied engineering and scientific disciplines including Mathematical simulations, Mechanical Engineering models, and Aeronautics and Astronautics system designs. With the wide array of cross disciplinary applications, modeling methods such as the Monte-Carlo (MC), Polynomial Chaos Expansion (PCE) and Proper Orthogonal Decomposition (POD) were developed to solve these problems. Unfortunately, these original methods are prohibitively expensive and have since received much attention to improve their efficiency. More specifically, the stochastic simulation of the Navier-Stokes equations through different computational methodologies is an active area of research. Although many improvements have been made to PCE and POD methods, many stochastic fluid flow problems remain computationally intractable. Thus, the most recently developed Dynamic Orthogonality (DO) method, developed by Sapsis and Lermusiaux (2009) from the MIT MSEAS group, is of great interest, since it promises to cut down computational costs by an order of magnitude or more for the same accuracy. The more efficient the fluid flow representations are with the same level of accuracy, the more engineers can utilize these simulation and design better fluid dynamical systems under a range of uncertain conditions.

This thesis is focused on examining the effects of the Reynolds Number on stochastic fluid flows behind a square cylinder and evaluating the DO methodology and computational

schemes to do so. This involves reviewing existing literature, examining our simulation results, and validating that our numerical solution is correct. The thesis uses a novel boundary condition formulation for stochastic Navier-Stokes equations (Ueckermann et al, 2012) which allows the modeling of a wide range of random inlet boundary conditions with a single DO simulation of low space-time dimensions. For this thesis, the range of inlet boundary conditions considered corresponds to variations of the Reynolds number, defined by $Re = \frac{\rho v D}{\mu}$, from approximately 20 to 100. This range contains two distinct laminar flow regimes: the lower-Reynolds number regime is steady and is characterized by a recirculation zone behind the cylinder, while the unsteady regime is characterized by vortices shedding at a frequency correlated to the Reynolds number.

Since the stochastic DO simulation is discrete, we evaluate the effect of different discretization parameters on the stochastic results. Specifically, to evaluate the approach, we first evaluate its accuracy, understand its constraints. Next, we can extend the approach or apply it to other problems. The numerical discretization of the continuous DO equations leads to discrete equations with matrices. One of the ways to evaluate the adequacy of the numerical code is to evaluate the convergence of the discretized simulations. In this thesis, we show that the new open-boundary stochastic modeling approach allows one to complete a large number of deterministic simulations with varied Reynolds numbers with a much cheaper single DO simulation with stochastic open boundary conditions. We also describe the dynamic global properties of the flow. We evaluate our dynamics result by comparisons with existing knowledge about flows behind a cylinder at varied Reynolds

number values. The key aspect of our application is that we can compute all of the solutions with a large ensemble of Reynolds number values with a single stochastic simulation.

Next we adjust the parameters to better understand their role in creating the realizations and how certain values will impact the convergence of the numerics. Convergence is important since we are modeling continuous equations with discrete time steps. At sufficient resolution, we should reach very close approximations of the governing fluid equations with parameter (Re) values described only by a probability density function.

Lastly, we calculate key characteristics of flows behind a square cylinder for mean Reynolds numbers within the interval 20-100. For that range of Re numbers, we find the recirculation zone length and vortex shedding frequency. The validation of this new method and calculation of key characteristics, like recirculation zone length and vortex shedding period, illustrates the possibilities of the new stochastic boundary condition approach we utilize. In the future, we can then transfer this knowledge to applications in different fluid test cases and in cross-disciplinary scenarios.

1.2 Background Literature

There is a large body of established literature on the topic of simulations and models of fluid flow around a cylinder. Within this literature, we found benchmarks which establish qualitative trends in the behavior of such flows. These trends are used to verify our unique approach to model uncertainty using our finite volume Navier-Stokes solver which uses the Dynamically Orthogonal method to predict probability densities of the flow. The fluid dynamics considered is that of flows around a square or circular cylinder in a

channel with a specified inlet velocity profile and boundary conditions. It has been observed that with increasing Reynolds number, the flow separates first at the trailing edges of the cylinder, leading to a closed steady recirculation region consisting of two symmetric vortices is observed behind the body. The size of the recirculation region increases with an increase in Reynolds number. When a critical Reynolds number is exceeded, the well-known von Karman vortex street with periodic vortex shedding from the cylinder can be observed from the wake. Based on experiments, Okajima (1982) found periodic vortex shedding at Reynolds number of approximately 70. Another value of 54 was found by Klekar and Patankar (1992) based on a stability analysis of the fluid flow. Separation at the leading edges has been found to occur between the bounds of Re = 100 to 150 by Okajima (1982) and Franke (1991). For a circular cylinder, this number is approximately 180.

Bruer et. al (1999) model laminar flow past a square cylinder using two numerical methods: lattice-Boltzmann and finite volume methods. For flows in the creeping steady flow regime, Re < 1, the flow past the cylinder persists without separation (Bruer 1999). For flows in the earlier parts of the laminar regime, Re > 1, for example Re ~20, we see a recirculation region (

Figure 1) consisting of two symmetric, vertically-stacked vortices in the wake. It is observed and proven that the length of this recirculation zone increases as the Reynolds number grows (Bruer 1999).

Bruer also found that the correlation between the recirculation zone length and the Reynolds number for the region between Re = 4.4 and Re = 60 is:

$$L_r/_D = -0.065 + 0.0554 * Re \qquad 4.4 < Re < 60$$

(eq. 1)

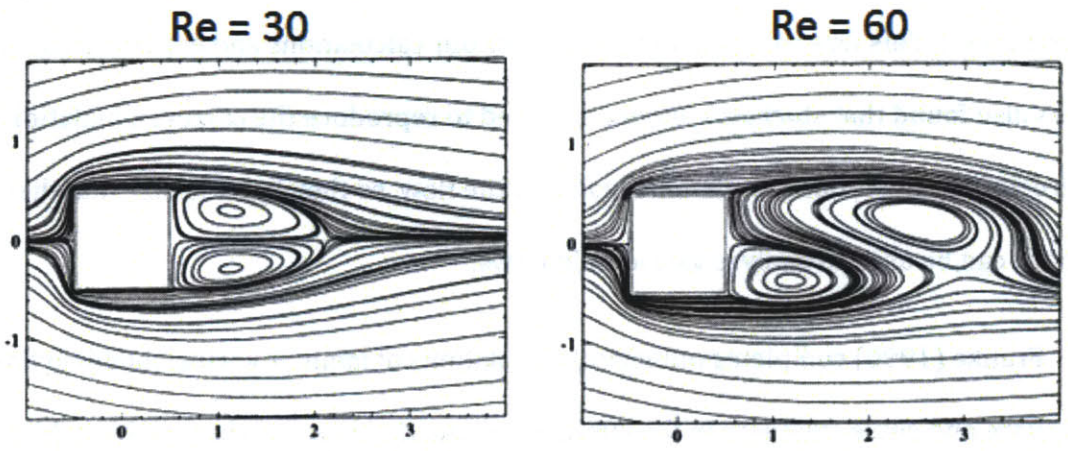

Figure 1: Recirculation Zone

At the higher Reynolds numbers, Re >100, there is the formation of eddies from the rollup of the free shear layers described as the von Karman vortex street as shown in the figure below (

).

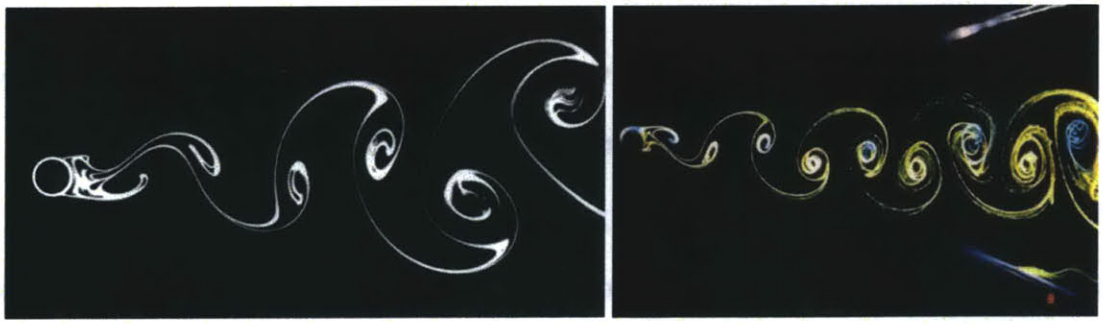

Figure 2: von Karman Vortex Street
Vortex shedding is longer and broader for the square cylinder than for the circular cylinder. This figure only shows the circular cylinder case. (Van Dyke 2002)

This pattern also has a frequency and it is observed that the period increases with rising Reynolds number (Davis et al. 1984). In Venturi (2008), they used an extension to

the proper orthogonal decomposition (POD) method to analyze a random laminar wake past a circular cylinder. Using stochastic eigen-decomposition and modal analysis, they suggests the shedding period for a circular cylinder to be roughly 6 convective time units (Venturi 2008). This was used as a benchmark for our calculations and experiments. The authors also found that stochastic modes required to reproduce the correct simulation are not directly dependent on the dimensionality of the flow, so they hypothesize that their approach can be used to analyze varied fluid flows.

Franke (1990) completes numerical calculations of laminar vortex-shedding flows past square and circle cylinders in the laminar regime. He observed that for Reynolds numbers below 150, separation occurs at the rear corners of the cylinder and the size of the vortices decrease as the Reynolds number increases to this threshold. However, at Reynolds numbers greater than 150, the opposite behavior is observed. The separation occurs at the front corners and the size of the vortices increase with increasing Reynolds number (Franke 1990).

Galletti (2003) employ the proper orthogonal decomposition to simulate multiple Reynolds numbers. The low dimensional modeling sets up the square cylinder symmetrically between two semi-infinite parallel walls. The inlet flow has a preset parabolic velocity profile and a set of boundary conditions to render the initial conditions consistent with the Navier-Stokes equations. They found that the numerical POD models are valid for certain Reynolds numbers and blockage ratio beyond the original investigations which includes Reynold number ranges from 60 to 255 and blockage ratio ranges from 0.125 to 0.375.

For a circular cylinder, shedding frequency can be found from modeling the lift force (Lin 2007). In that manuscript, the author modeled stochastic simulations of compressible and incompressible flows using the Polynomial Chaos method. Incorporating the randomness of the stochastic inlet velocity, he found an empirical relation between the Reynolds number and vortex-shedding frequency. He found that for the range of Re, [90, 100], the shedding frequency, f_s, varies linearly between [0.1592, 0.1697]. The author concluded that that the analytical solutions found verify the numerical methods developed in the paper. We can use all of these results as benchmarks for our square cylinder case study.

Lastly, Sharma described the previous findings on the Re_{crit} values for flows and their blockage ratio (Table 1). This is used to benchmark our results since there hasn't been a definite answer to the value of the Re_{crit}. The answer is heavily influenced by the initial dynamic conditions of the flow like Reynolds number, and also by the Prandtl number and Strouhal number.

Table 1: Previous Re_{crit} findings in existing literature

Author	Re_{crit}	Blockage ratio	Leading or Trailing edge at high Re (Re <150)	Leading or Trailing edge at very high Re (Re >150)
Kelkar et. al.	54	14.3 %	.	.
Norberg	47	~0 %	.	.
Sohankar et. al.	51.2	5 %	Trailing edge	Leading edge
Franke	.	8.3 %	.	Leading edge
Robichaux	.	5.56 %	Trailing edge	Leading edge

1.3 Dynamically Orthogonal (DO) representation of Stochastic Navier-Stokes Simulations

Fundamentally, the Dynamically Orthogonal representation is a decomposition of the Stochastic differential equations, in our case the Navier-Stokes equations. To fully represent the randomness of a discretized field, each point on the grid would require its own random variable. However, DO takes advantage of the assumption that if the flow is sufficiently continuous, then we may be able to obtain accurate estimates on the velocity and energy states at a point on the grid deduced from what we know about the nearby grid points. To put it simply, the velocities are correlated to each other. This intuitively makes sense because in fluid flows, for the liquid to move from one position to the next one, it must affect the nearby liquid, just by local conservation of mass and momentum.

DO uses the following discrete decomposition:

$$u(x,t;\omega) = \bar{u}(x,t) + \sum_{i=0}^{s} u_i(x,t) y_i(t;\omega) \qquad \text{(eq. 2)}$$

The variable u is the stochastic velocity. It can be decomposed into two parts, the mean and sum of the stochastic modes times the coefficients. The variable $\bar{u}$ is the average velocity. The variable u_i represents the velocity-field for a single random variable on the grid based on how the local velocities are affected by that random variable, and y_i is the stochastic coefficient, which is a realization of that random variable. The $\sum_{i=0}^{s} u_i y_i$ term is the sum of all the stochastic aspects of the flow. Depending on the magnitude of$s$, the number of "DO helper modes", we can realistically model stochastic fluid systems.

To further understand, we can take a close look at the last term incorporating the randomness. This sum of products is broken down in two factors: u_i and y_i. The u_i represents the orthonormal basis of the portion of the velocity field that is random; it is a field that can range in values over the spatial domain. The values for this variable depend on the dynamics of the flow, time and spatial constraints, and the boundary and inlet conditions of the system. The y_i's are the stochastic coefficient for each mode. Depending on the value of these stochastic coefficients, y_i, which is described by a probability density function, we can obtain diverse results for the direction and magnitude of the velocity. For example,

plots the 1D projected (along the diagonal) and 2D projected scatter plots of realizations for the base case examined, and this shows the complexity of this 10-dimensional probability space (Ueckermann and Lermusiaux, personal communication).

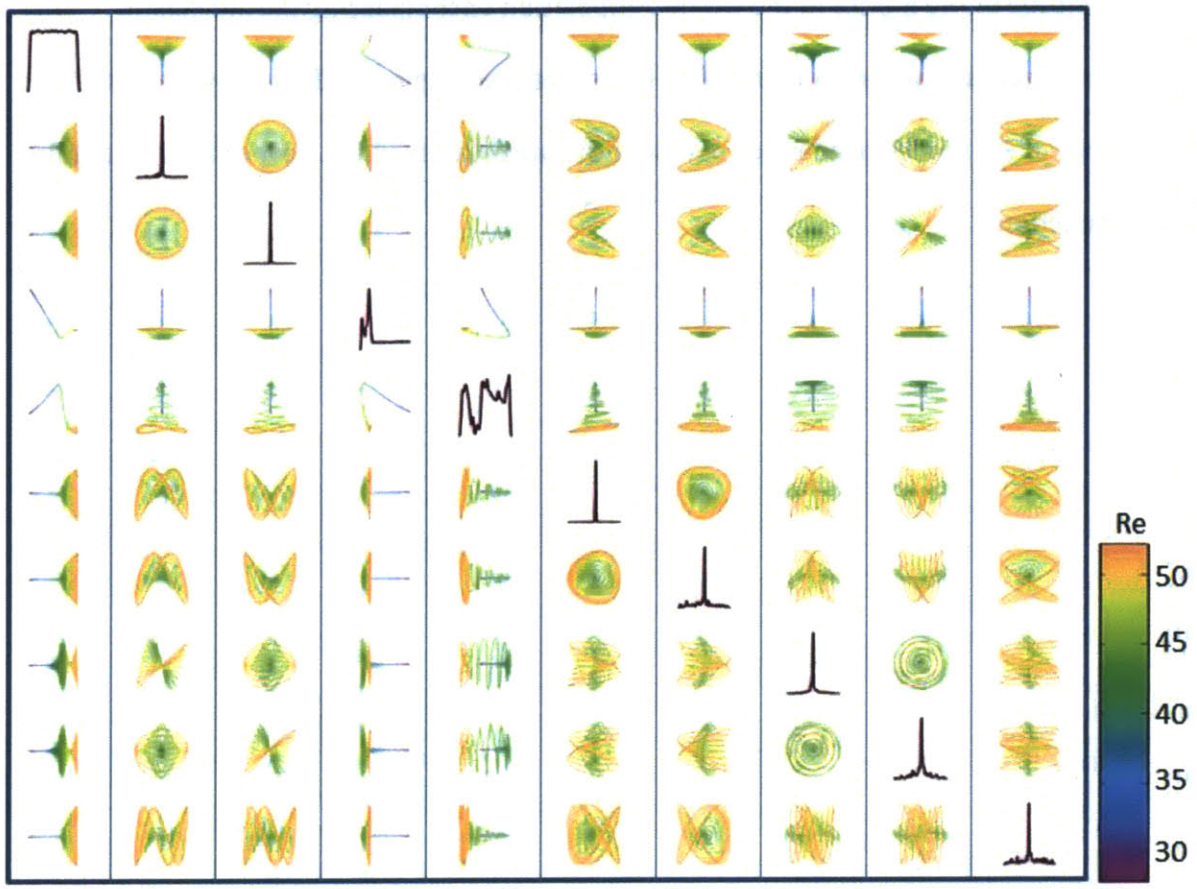

Figure 3: Graphical Representation of Stochastic Coefficients.
The 1D projected (along the diagonal) and 2D projected scatter plots of the realizations of the stochastic coefficients, y_i's. The coefficient realizations are colored by the corresponding Reynolds number (Ueckermann and Lermusiaux, personal communication).

As illustrated on

, the magnitude of the modes in the DO decomposition encompassing the stochastic coefficients decrease as the mode number increases (see Figure 4). This allows one to limit the number of DO modes needed to represent the uncertainty in the flow or its probability density function.

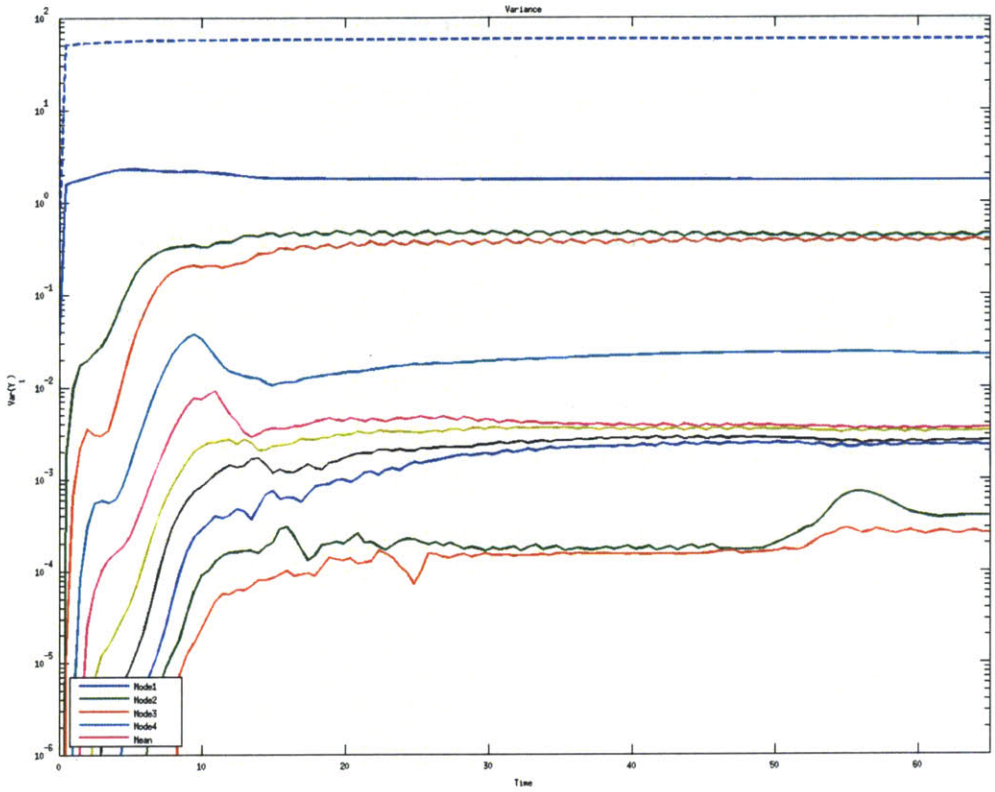

Figure 4: Magnitudes of Mean and Modes
The dotted line is the magnitude of the mean, and the next five lines show the amplitude of the first 5 modes.

If, at a particular point in time, we take a single, 10-dimensional point from

Figure 1, multiply each dimension by its corresponding mode, sum up all of these (so, essentially a dot-product), and add the mean velocity, we can construct a deterministic realization of the field. However, in the above results we only showed the DO decomposition, that is the mean and the first five modes, as the final output for each time step. To illustrate realizations proper, Figure 6 shows the DO decomposition on the left, and 5 deterministic realizations at different Reynolds numbers for the base simulation.

The number of DO modes necessary, that is, the value of s, to accurately model a range of different dynamics depends on the complexity of the flow (Sapsis and Lermusiaux, 2011). Based on the expected flow behavior at the Reynolds and Strouhal numbers for the flow we are studying, we can make a good approximation for how many DO modes are necessary to reach convergence for our numerical simulation. For larger Reynolds numbers, it is expected that more DO modes will be needed. While we can make a good approximation of the number of DO modes needed, this thesis dives deeper in testing the boundaries of DO and understanding its effectiveness.

2. Model set up and Validation

The deterministic version of the Navier-Stokes code used has been extensively verified with standard CFD test-cases. The Stochastic version, in turn, was validated against this deterministic version (Ueckermann et. al. 2012). However the new stochastic boundary conditions (Ueckermann and Lermusiaux, pers. com.) have not been previously validated and this is one of the goals of this thesis. To validate this, we examine a particular flow setup, described next. To ensure that this setup was accurately modeled, we varied several numerical discretization parameters, but each time only one at a time. By both increasing and decreasing the resolution of the discretization, we could examine whether the results converged. Since many of these test runs were the same as those used in the results presented in the next section, excepted that their objective was to validate the numerical model and open boundary condition methodology, we present all the results in the next section. In addition to those tests, we also ensured that the base simulation was repeatable given different realizations of the stochastic coefficients.

We also wanted to study the effect of different flow and dynamical model parameters. In this thesis, we will focus on the flows behind a square cylinder. Our objective was to create a similar test case setup to those we found in the literature. For example, we set a uniform inlet boundary condition for the velocity. We also used a no-slip condition for the fluid around the cylinder, while using a slip condition at the top and bottom boundaries. We had the choice between a square or circular cylinder, but chose the latter because we could accurately represent a square cylinder using a structured grid. Lastly, we chose to study two-dimensional flows (see Figure 5 for a summary).

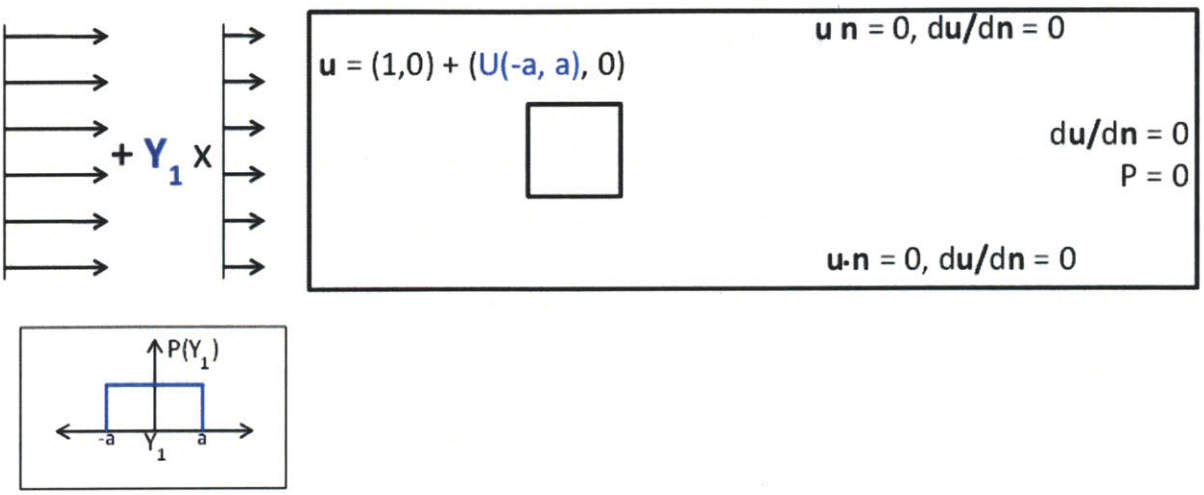

Figure 5: Square Cylinder Model of the test scenario

To define the flow characteristics for the stochastic simulation, we had to set the Reynolds number and Reynolds number range. Specifically, it is the uncertain inlet boundary condition that leads to a variable Reynolds number. Since the behavior of the flow drastically changes depending on the Reynolds number, it was important to capture all of this variation within a single DO simulation. This was possible because the random realizations of the inlet boundary velocity are mapped uniquely to the stochastic subspace, in the form of stochastic coefficients that are defined in that subspace. This is a key of the new boundary condition approach. It allows representing simulations over a wide range of Re numbers with a single DO simulation. Numerically, the randomness is modeled by taking a large number of Monte-Carlo samples from MATLAB's pseudo-random number generator for uniform distributions. Of course, the realization in the subspace can also be re-mapped to the physical space, as illustrated in Figure 6 for five different Re number values.

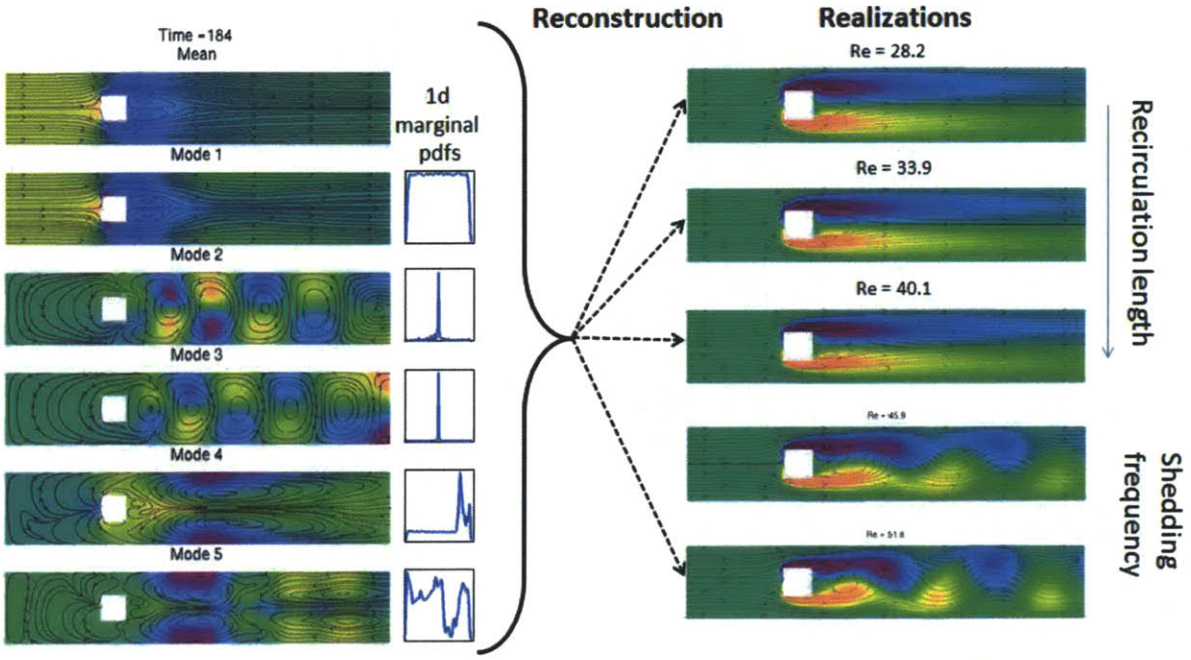

Figure 6: Mean and first 5 modes of DO Decomposition (left) and reconstruction of 5 deterministic realizations (right).

During our study of stochastic fluid flows past a square cylinder, we wanted to evaluate how well our new method could capture multiple dynamical regimes in a single simulation. For this, we needed to better understand how the numerical discretization of the stochastic fluid flow equations affects the behavior of the solution. Understanding how discretization errors behave is important for any application, not just the flow we studied.

3. Understanding the Parameters of DO

3.1 Experiment Setup and isolation of parameters

After we verified the model, we are able to set up cases. Each simulation is ran to a non-dimensional time of 65, which would allow the fluid to travel approximately 4 times the size of our domain. We save snapshots of the solution at every half-unit of non-dimensional time, for a total of 130 snapshots for analysis. For the initial case, also referred to as the base case or original case, we chose the optimal numerical parameters, i.e. parameters that led to what we deemed "good" results by comparisons with the literature but also by numerical convergence analysis for the stochastic DO simulation. From the latter results, we concluded that the simulation had converged, or in other words it provided a reasonably accurate numerical solution of the Navier-Stokes Equations and had acceptable errors at the boundaries. These results are presented next.

We implemented numerous test cases to understand how the simulation will behave if we change the key input parameters to the stochastic simulations. The main inputs that determine the flow characteristics and accuracy of the simulation consist of Reynolds number (Re), number of Monte Carlo samples (MC) in the subspace, number of spatial points (N), and number of "helper" DO modes(s). The Reynolds number determined the flow characteristics of the test and we expected to see significant changes in flow behavior as we adjusted its value. The number of Monte Carlo samples helped us represent the probability density function of the randomness we wanted to capture for our problem. Therefore, we expected changing the Monte Carlo samples to affect the shape of the probability density functions. The number of spatial points determined the spatial

resolution of the simulation. The size of the domain for our test is three units high by sixteen long in non-dimensional spatial distance, but the number of finite volumes per these unit blocks is controlled and determines the numerical resolution. We expected the higher the resolution, the "cleaner," or more accurate the results in terms of paths for streamlines, eddies, vortices and recirculation zone. Lastly, the "helper" DO modes are instrumental in capturing the variation due to the uncertain inlet boundary condition, or uncertain Reynolds number. We expected that changing the number of DO modes would change how well we capture the dynamics at different Reynolds numbers.

The original case that converged was optimized manually to achieve the most accurate result in the shortest computational time by using heuristic methods. The original case we arrive at has the parameters listed in Table 2, and the result is illustrated seen in

. Importantly, we note that the base case corresponds to a single DO simulation but actually represents 10^5 deterministic simulations.

Table 2: Original Parameters for the Base Case

	Mean Reynolds	Range of Reynolds Numbers	Monte Carlo Samples	No. of Spatial points	Observation Time step	No. of DO helper modes
Base Case (Case 2)	Re = 40	Re_span = 0.3	MC = 10^5	N=15	T=65	S = 9

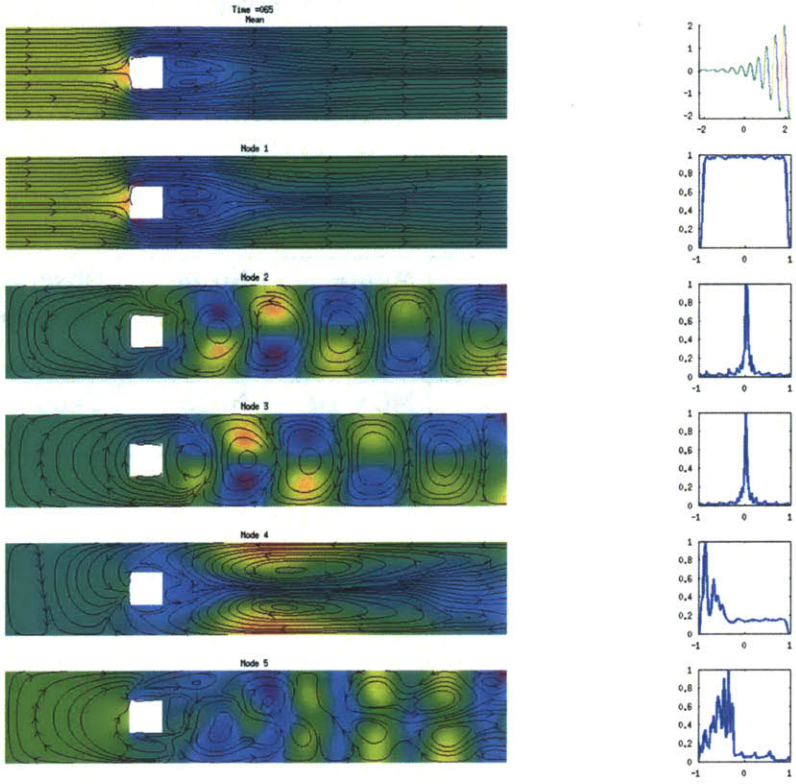

Figure 7: Mean and first 5 DO Modes and marginal pdf's of the Base Case. The top right plot shows the 2D projected scatter plot of Y_1 (x-axis) and Y_2 (y-axis).

Using this initial case as the control, we adjusted one of these parameters in each of the following cases. The simulation results differ depending on the parameter change. The parameters that are varied between runs can be seen in Table 3 and Table 4, along with a qualitative description of the effects compared to the base case. In Table 3, the changes in Reynolds number mean and range, and the number of Monte Carlo is examined. In Table 4, the changes in spatial resolution and number of DO modes is examined.

Table 3: Test Cases Observation Table: Reynolds number and Monte Carlo Samples.

	Base Case (Case 2)	Low Reynolds No. (Case 3)	High Reynolds No. (Case 4)	Low MC Samples (Case 5)	High MC Samples (Case 6)
Variable of interest	.	Re & Re_span	Re & Re_span	MC	MC
Parameter of interest	.	Reynolds number and range of Reynolds Numbers	Reynolds number and range of Reynolds Numbers	Monte Carlo Samples	Monte Carlo Samples
Value of parameter	.	Re = 20 Re_span = 0.60	Re = 60 Re_span = 0.67	$MC = 10^4$	$MC = 10^6$
Observations of simulation	.	Larger eddies and less uniformity, lack of symmetry	4^{th} and 5^{th} mode have much finer structures	Modes reverse eddies direction, and chaotic streamlines.	Same.
Observations of pdfs	.	Straight curves. Odd profiles asymmetric.	Larger Amplitude. Very symmetric.	Profiles have less resolution	Mode 1 has slightly smoother curve

Table 4: Test Cases Observation Table: Spatial points and DO helper modes.

	Base Case (Case 2)	Low Spatial Points (Case 7)	High Spatial Points (Case 8)	Low DO Helper Modes (Case 9)	High DO Helper Modes (Case 10)
Variable of interest	.	N	N	S	S
Parameter of interest	.	No. of Spatial points	No. of Spatial points	No. of DO Helper modes	No. of DO Helper modes
Value of parameter	.	N = 10	N = 20	S = 5	S = 13
Observations of simulation	.	Same. Except for divergence in modes 2 and 3. Mode 5 is incorrect.	Simulation is more refined with the same curves and streamlines.	Mean and modes vary significantly from base case. Eddies occur in different positions and the streamlines are incorrect in later modes.	Models have different pressure densities and streamline patterns. Eddies differ in size but the shape stays constant.
Observations of pdfs	.	Same	Same	Probability density function are much more coarse and choppy	Same but differ in higher modes

3.2 The test cases and their results

Sensitivity of the stochastic DO simulation to the Reynolds number: In the first parameter changing pair of test cases, we look at adjusting the Reynolds number. Because the inlet velocity conditions are set, we are able with this model to adjust the mean Reynolds number of the flow thus changing the dynamics. The first case, we adjust the mean Reynolds number to twenty (

) and the latter case, we adjust the Reynolds number to sixty (

). Along with this adjustment of the mean, we have to change the Reynolds number range (Re_span). The span of the Reynolds number is equal to plus or minus twenty for the base case, but changes need to be made for the new mean Reynolds numbers. We desire the upper bound Reynolds number for the low Reynolds number case to equal the base case (Re = 40) and the lower bound for the high Reynolds number case to also equal the base case (Re = 40) so we have a continuous spectrum. A range of twenty for the low Reynolds number case would have equated to zero on the low end, meaning there is no flow which is not helpful for our study. For the lower boundary, we fix the lower span to be 8 so the Re_span became 0.6 rather than 0.3. For the high Reynolds number case, we could succeed in making the lower bound of 40 to be included so we changed the span to two thirds.

After running the simulation, we see the low Reynolds number case shows very different flow patterns in comparison to the base case. The mean has a smaller recirculation zone length, and the first five modes are significantly different. The fifth mode for the low Re case resembles the third mode for the base case (but with a dominant signature at the outlet boundary), while the first four modes are more similar to the fourth mode in the base case. This is as expected, since the low Re case does not contain realizations with vortex shedding. For this case, the pdfs are also vastly different, with curves seeming smoother, without the single sharp peaks as in the base case.

We see that the high Reynolds number case exhibits the same flow direction, but with denser streamlines, irregular eddies, and possibly more vortex shedding. In particular, modes four and five are significantly different from the base case, showing much finer,

vortex-shedding structures. This is expected since every realization from this case exhibits the recirculation-zone dynamics. In addition to the actual means and modal portions of the simulation, we can also comment on the mode-by-mode marginal probability density profiles. The two higher Reynolds number cases show significant differences in the shape of the marginal profiles for the modes, especially due to oscillations. They indicate the nonlinear (non-Gaussian) behavior in the stochastic subspace, where the non-marginalized probability densities are not uniformly distributed. In other words, the different Re numbers lead to a single curve in that space, but that curve is organized in the space (it does not randomly cover the whole space). Of course, if we recombine all of the modes together, we recover the original uniform probability density, up to numerical errors.

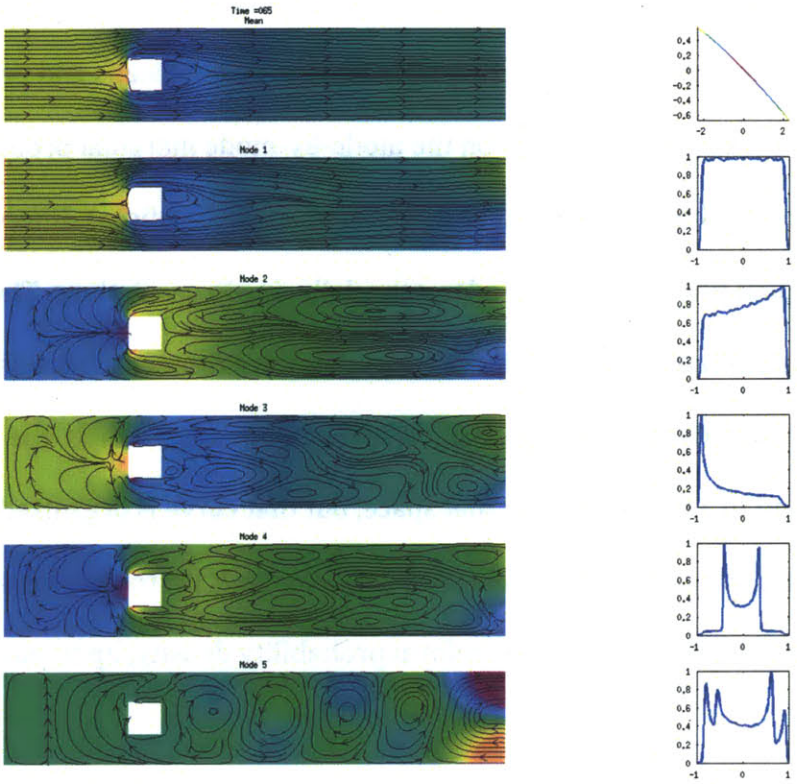

Figure 8: Low Reynolds Number (Cases 3)

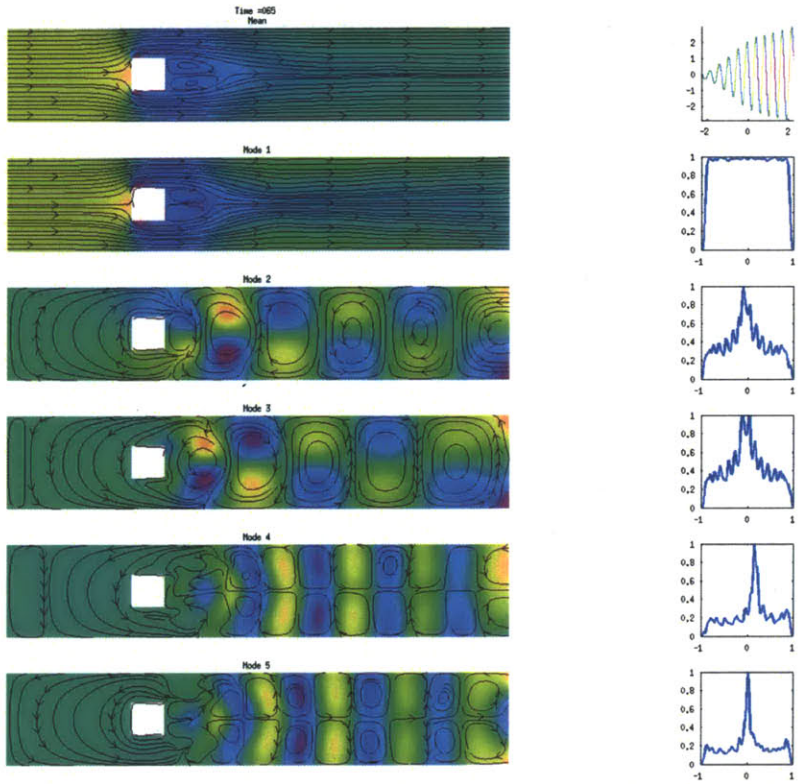

Figure 9: High Reynolds Number (Case 4)

Both the low and high Reynolds number cases vary from the control case in their streamline structure and how the stochastic profiles impacts the flows. The Reynolds number, by definition, should impact the dynamics of the flow and how it will react to the square cylinder obstacle.

Sensitivity to the Stochastic Resolution: The next parameter for analysis is the impact of the number of Monte Carlo (MC) Samples in the stochastic subspace. For this stochastic simulation, the number of samples dictates the randomization and repeatability of the results so it is important to inspect how this quantity impacts the resulting realizations. In

similar fashion to the Reynolds number trial cases, we increased and decreased the number of Monte Carlo samples on the simulation and probability profiles. The results are shown in

and

, respectively. To do this, we changed the Monte Carlo input value.

The results are very interesting. In addition, the realization in mode four shows a different set of streamlines, in thickness, proximity, and direction. The higher Monte Carlo samples displays results almost identical to the base case, confirming convergence. However, the streamlines in two and five have noticeably more streamlines. There are also slightly different pressure gradients. The higher MC case also has higher pressure peaks than the base case. In addition, it is important to note that these plots do not necessarily show a clearer or higher resolution.

Of course, if we vary the number of sample, we can mainly expect variations in the profile of the density function. Interestingly, the profiles for the higher MC case are very similar to those of the base case, again showing convergence. The profile for mode 1 is closer to a uniform one, as expected. The other marginal for higher modes remain very similar, still showing the same peaks, indicative of the very organized (and non-uniformly distributed) sample curve in the stochastic subspace. For the former lower-resolution case, the marginal profiles have noticeably less resolution, but have overall similar shapes..

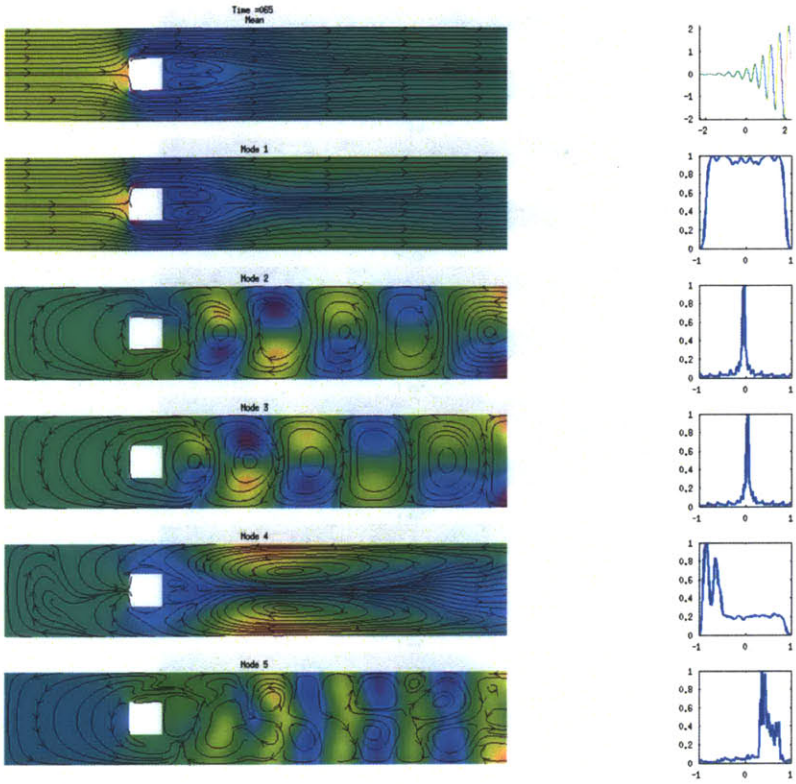

Figure 10: Low Monte Carlo Samples (Case 5)

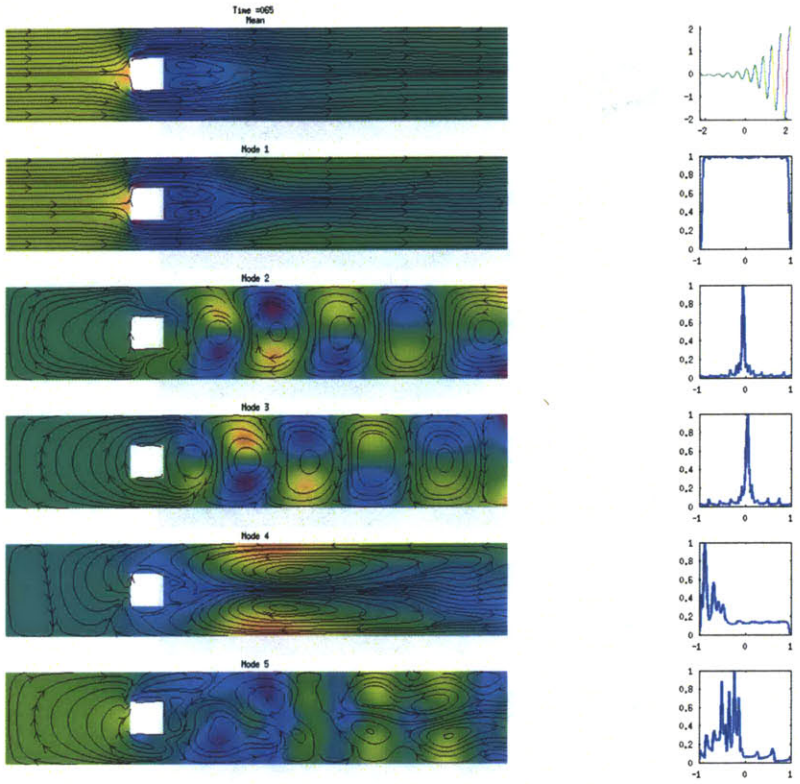

Figure 11: High Monte Carlo Samples (Case 6)

Sensitivity to the Spatial Resolution: The next parameter we studied is the number of spatial points. We set up our finite-volume grid in a similar fashion to that of simulations employed in the literature. In our 3 by 16 non-dimensional unit spatial blocks, we have to divide each block in a number of discrete finite-volumes. This drastically affects our computational cost and simulation run time. The goal is to see how an increase or decrease in this mesh size resolution affects the result of our simulations.

For the two test cases dealing with spatial points, we change the number from of finite volumes per unit distance from fifteen to ten for the lower bound (

) and twenty for the upper bound (

). This implies that we vary the total number of finite volumes from (15x3 by 15x16, i.e. 45 by 240) to (10x3 by 10x16, i.e. 30x160) for the coarser simulation and to (20x3 by 20x16, i.e. 60x320) for the higher resolution. In the lower resolution case, we observe the pressure gradient becomes opposite in mode two but then corrects itself in later modes. This is not relevant because if the pressure or velocity in the DO modes is flipped, then the probability density function will also be flipped. Mode three shows small deviations from the base case in terms of streamline path. Mode four shows a possible re-convergence to the base case model and in the last mode of the figure, mode five, the graphic displays a clear streamline divergence. That is, the result of mode 5 diverges from the base case, which seems to indicate the spatial resolution is insufficient. For the latter higher-resolution case, the modes looked more refined with the same curves and streamlines. However, they are similar to that of the base case.

When observing the marginal probability density profiles, we see that they nearly look exactly equal to these of the control test run. The lower spatial resolution case exhibits an exact copy of the profiles for the first four modes; however, in mode five, there is a sharp contrast. For the higher spatial resolution, the profiles are in line with the original test case, indicating convergence of the marginal densities with respect to the spatial resolution in the physical domain.

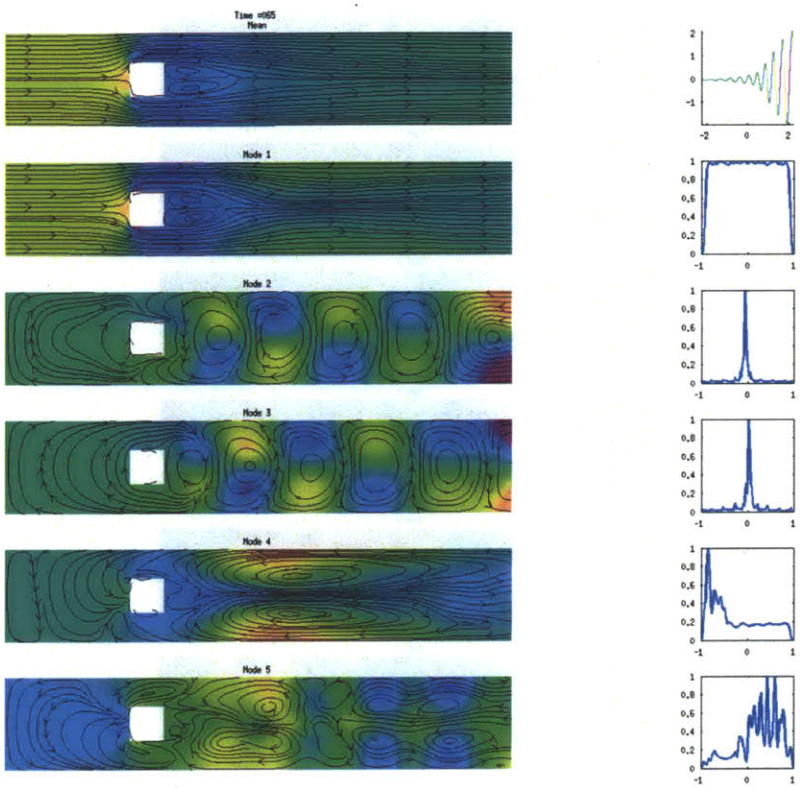

Figure 12: Low Number of Spatial Points (Case 7)

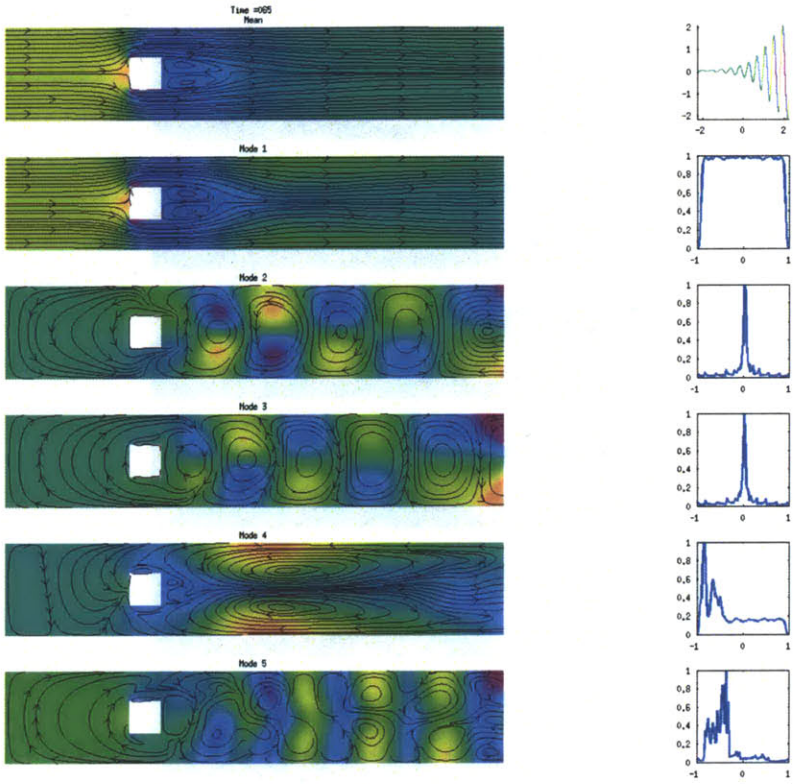

Figure 13: High Number of Spatial Points (Case 8)

From these spatial resolution studies, we can conclude that the spatial resolution does not alter significantly the dynamics of the simulation but change its details. The lower resolution causes the simulation to diverge in the fifth mode so the accuracy of the stochastic simulation is not sufficient for the five modes. For the larger number of spatial points, we obtain a higher similarity with our base case simulation; there is not much added information from this increase in mesh size. Thus we conclude that using 15 spatial points gives a sufficiently accurate solution.

Sensitivity to the number of open boundary condition DO modes: In the last parameter investigation, we examine how the number of Dynamically Orthogonal (DO) helper modes affects the simulation. The DO helper modes are the stochastic summations needed to represent uncertain open boundary conditions. Each mode represents a stochastic velocity basis. A realization consists of a combination of the mean velocity, velocity modes and sample realizations of the stochastic coefficients which is defined by the probability density function (pdf). There are nine DO helper modes in the initial test case to encompass all of the randomness. We examine two deviations in similar fashion to the previous parameters. The low number of DO helper modes is five (

) and the high number of DO helper modes is thirteen (

).

The results of the simulation for the low number of DO helper modes show the mean and modes varying significantly from the base case. Eddies occurred in different positions across modes. For example, the modal streamlines and eddies differ in size and direction in modes two, three and five. In particular, due to the orthogonally constraint and some variations in the mode shapes, it seems as though the order of modes two and three are switched, and mode five has finer-scales than observed in the base-case. The reason for this change in vortices size is that with only five modes, each helper mode needs to encompass more of the dynamics, but they can only do so approximately. If we consider the marginal probabilities, we find that the marginal probability density functions are affected by the decrease in the number of DO helper modes. We note that since we used a consistent set of randomly generated numbers, the differences in marginals are only due to the lack of sufficient modes.

The case with a higher number of DO helper modes has marginal profiles that are more similar to that of the base case. The higher DO helper modes are similar to the base case, but begin to differ from the base case at mode five. Mode five has much more symmetry and it is evident that there are more modes describing more complex dynamics, like vortex shedding that is not shown here. The base case seems to have finer-scale structures than the higher mode case, and the higher-mode case is also more symmetric. Since there are many more modes in this case, we are not seeing the whole decomposition but we can infer that the more modes available, the more accurate the decomposition of the

stochastic simulation can be. Each mode takes on less of the dynamics in the case with a higher number of DO modes.

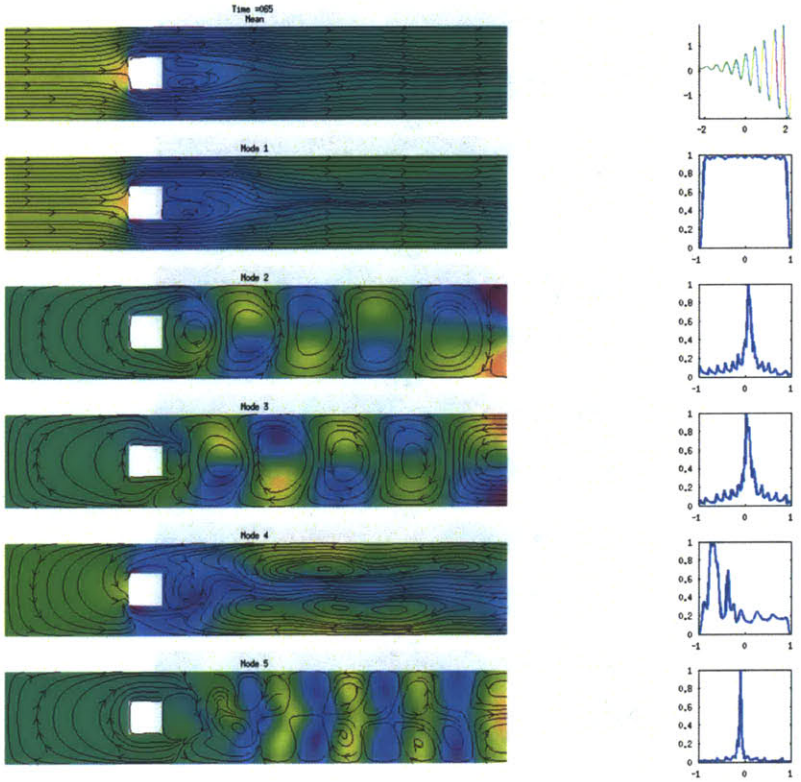

Figure 14: Low number of DO helper modes (Case 9)

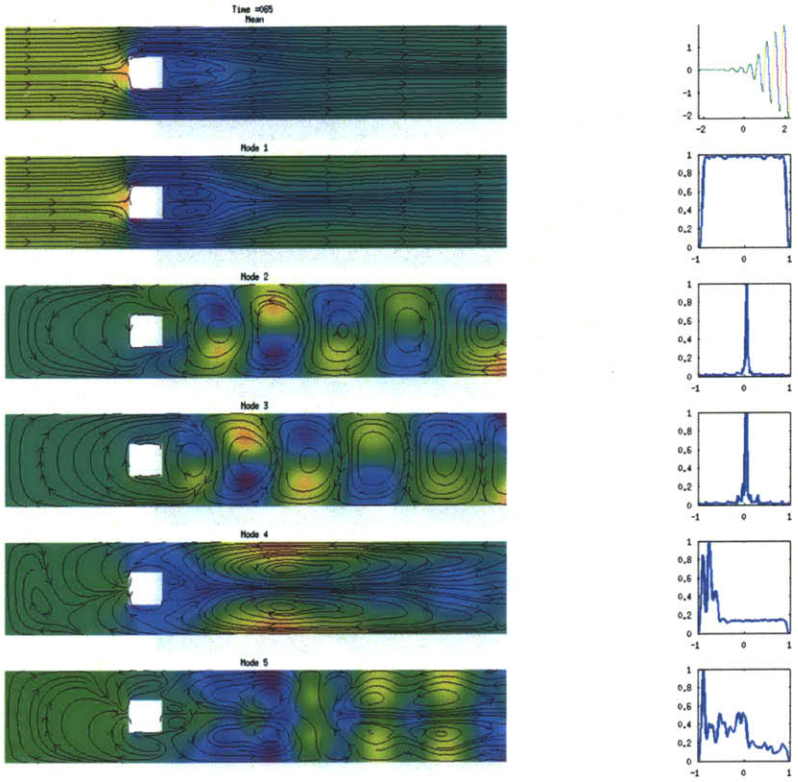

Figure 15: High number of DO helper modes (Case 10)

What do the above results mean? Since the DO helper modes create the decomposition of the actual simulation, the order and patterns play a large role. The level of complexity of the system determines the amount of DO helper modes needed. For example, for low Reynolds numbers, the mean velocity is very small so the higher DO helper modes will have limited effects of the final realizations since the slow flow isn't as dynamic. We also realize that the number of DO modes affects how much of the dynamics can be described with each mode. In some sense, the higher the number of DO modes there are, the more the dynamics can be broken down in each mode. The coefficients are also linked to the number of modes so this number affects the stochastic dynamics in the

subspace as well. However, since we plotted coefficients that are scaled (normalized) by the magnitude of the total perturbation of the u_i velocity term, the smaller the u_i or slower and less complex flows, the less the stochastic coefficients actually plays role. All in all, we can deduce that the more complex the flow, the more DO helper modes are needed for a proper stochastic representation. It seems as though the higher DO mode case better separates the different dynamics of the flow in mode 5, and it would suggest that we could obtain better results using more DO modes. However, for our purposes, these are similar enough to the base-case (since the contribution from the 5^{th} mode is 4 orders of magnitude smaller than that of the mean).

3.3 Summary

In summary, we obtained optimal parameter values for our flow of interest by bracketing of values, adjusting of each value until the control case was similar to the case with higher resolution in the physical space, stochastic space or stochastic dimension. Out studies focused on mean Reynolds numbers between twenty and sixty because this allows for some dynamics develop, requiring several DO helper modes. The number of Monte Carlo samples is optimized at one hundred thousand samples (10^5) because this shows all the detail of the simulation without becoming too computationally expensive. Additional increase in Monte Carlo members did not add much more information. The number of spatial finite-volumes is optimized in this setup with fifteen volumes per unit distances in non-dimensional terms. Additional increase in mesh size does not add much more information. We also understood through heuristic methods that the less spatial points we used, the less accurate our simulation became. For number of DO helper modes, nine was

chosen for our dynamics since additional modes did not alter the modes 1-to-5. Such comments are qualitative versions of the quantitative criterion employed in Lermusiaux (1999) for evaluating convergence of the stochastic subspace.

4. Determining and Calculating New Dynamical Characteristics

4.1 Recirculation Length

After understanding the inputs, limiting factors, and capabilities of our single DO stochastic simulation, we used it to calculate key characteristics or properties of the fluid flow: the recirculation length and vortex-shedding frequency. As described in past literature, the recirculation length is characterized by the initial separation of the flow at the trailing edges of the cylinder and the formation of two closed and steady symmetric vortices.

To calculate the characteristic recirculation length for a specific mean Reynolds number, we can monitor the horizontal velocities along the center line at a single point in time. Assuming the recirculation zone occurs directly behind the cylinder and that the Reynolds number is in the appropriate regime, the horizontal velocities should be toward the cylinder (opposite to the inlet velocity direction) when inside the recirculation zone. However, after reaching the end of the recirculation zone along the center line, the direction of the horizontal component of the velocity should change. If we track the position on the grid where this change of sign or direction of the horizontal velocity component occurs, we can estimate the recirculation length.

Below we have four cases where we calculate the recirculation zone length. These cases vary the Reynolds Numbers: Re = 20 (Case 3), 40 (Case 2), 60 (Case 4), and 110 (Case 11). We refer to these cases as low Reynolds number, Mid Reynolds number, High Reynolds number, and very High Reynolds number.

For the low Reynolds number case, we see an upward trend in the recirculation zone length (Figure 16). It increases linearly from slightly less than one non-dimensional unit distance to slightly over 1.6 non-dimensional spatial units. Also, the slope is 0.0537 with a covariance of 1.24×10^{-6} and standard deviation of 0.0011. The covariance and standard deviation is from possible error since the slope is calculated by averaging the slope between numerous points on the line. This positive slope agrees with previous literature, e.g. Bruer also found that the recirculation zone length increases with the increase in Reynolds number, after Re = 5, passing the creep zone.

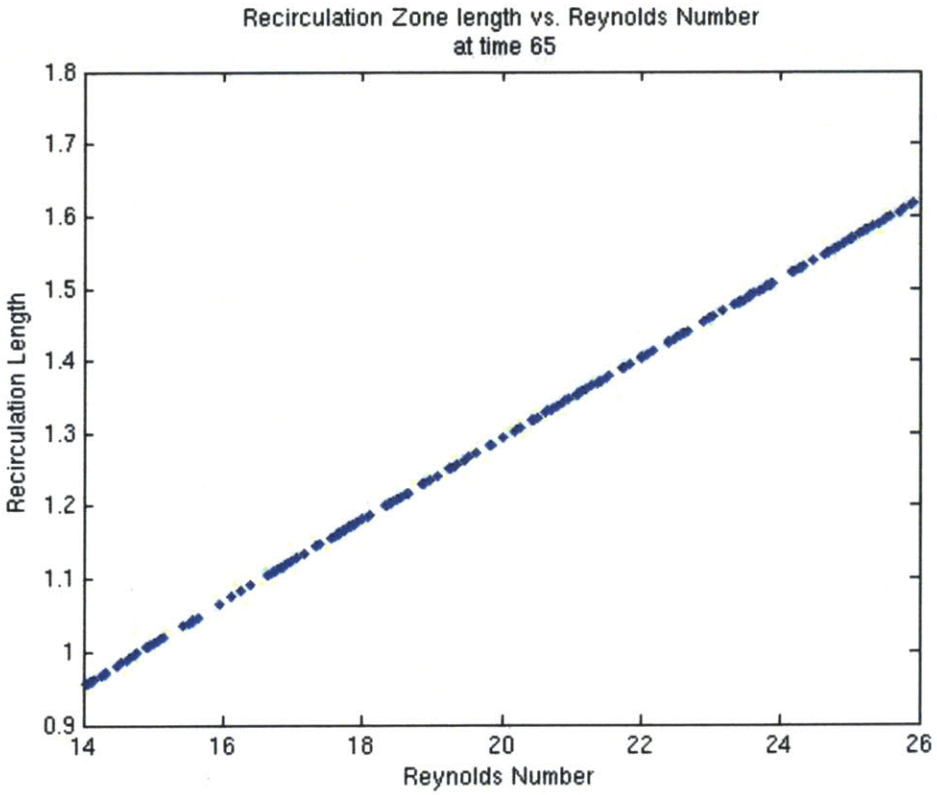

Figure 16: Low Reynolds Number, Non-dimensional Recirculation Zone Length (Case 3)

For the mid Reynolds number case (

), we see an upward trend, a peak, and then a decline in the recirculation zone length. It increases from slightly more than one 1.8 non-dimensional unit at Re = 30, peaks a little after Re = 40, then declines. The curve is no longer linear (there are changes in slope and curvature). In the subplot below showing the decline, the curve loses its definitive linearity. This makes intuitive sense because at this Reynolds number regime, we begin to see the onset of the vortex shedding and it no longer makes sense to find the edge of a steady recirculation zone because of the periodic separation. The slope of the line from Re = 28 to Re = 42 is 0.0553 with a covariance of 7.65×10^{-5} and with standard deviation 0.0087. However, it is the same slope as in the low Reynolds number case which we expected to hold true, further validating the DO simulations with our new open boundary condition formulation.

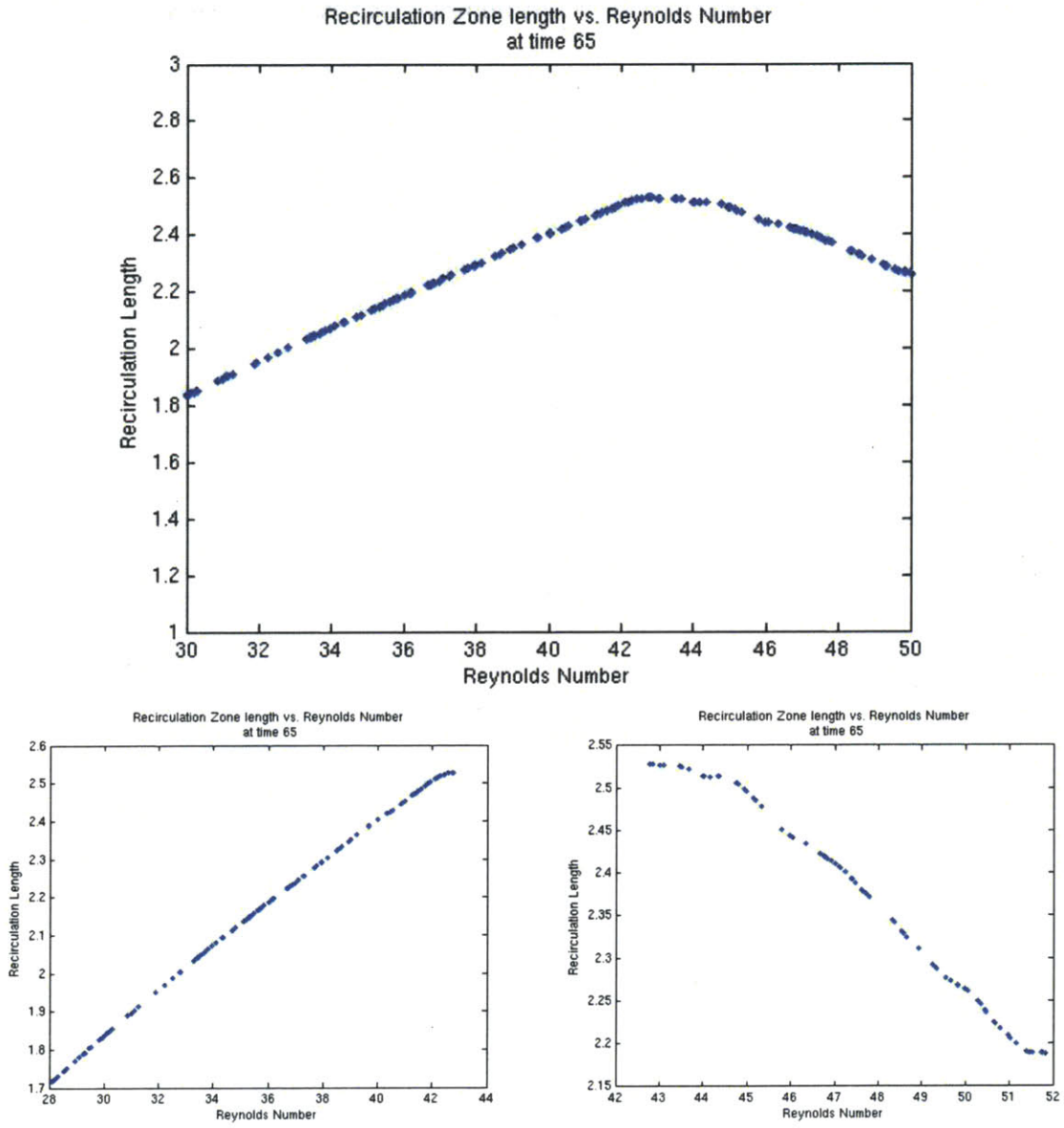

Figure 17: Mid Reynolds Number, Non-dimensional Recirculation Zone Length (Case 2).

Next we can analyze the recirculation zone length in the high and very high Reynolds number cases (

Figure 18 and

). Here, we continually see a decline; however, the slope is very far from being linear. The reason for this, as discussed in the mid Reynolds number case, is the vortex shedding, which is very apparent. In the very high Reynolds number case (

), this is especially clear. The slope for the high and very high Reynolds number cases respectively were, -0.0408 and -0.0139. However, the covariance and standard deviation were two and one orders of magnitude larger than the low Reynolds number case. This once again makes sense because the recirculation zone length does not hold for high Reynolds numbers. This makes the slopes irrelevant because this behavior is not exhibited. Therefore, these slopes, covariance, and standard deviation values are not included in Table 5.

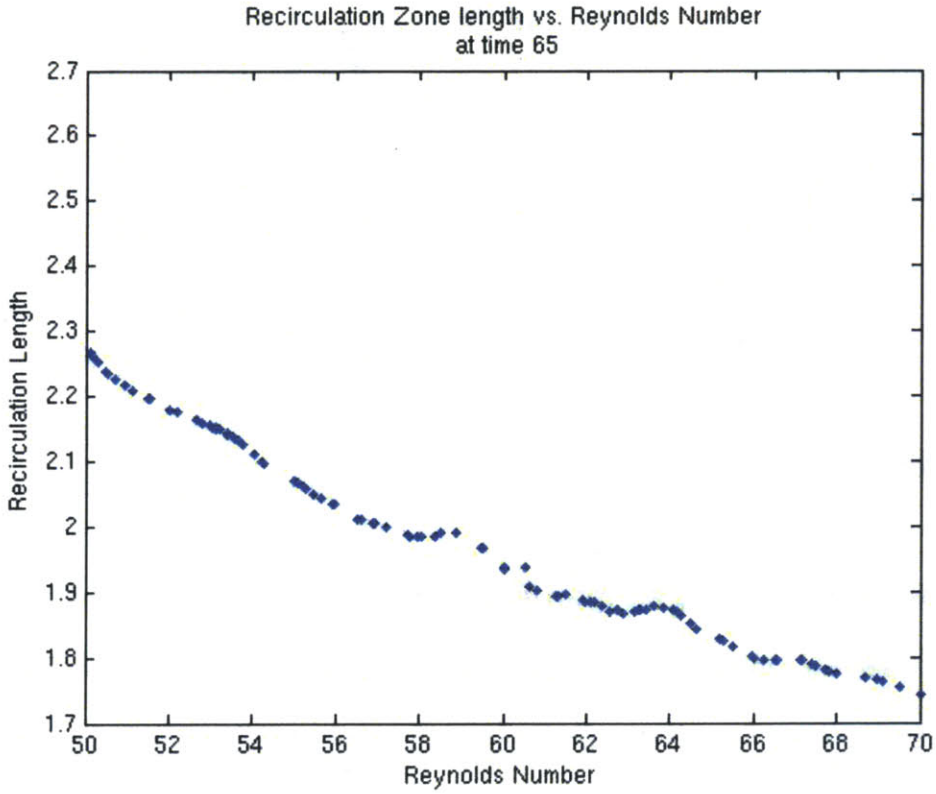

Figure 18: High Reynolds Number, Non-dimensional Recirculation Zone Length (Case 4)

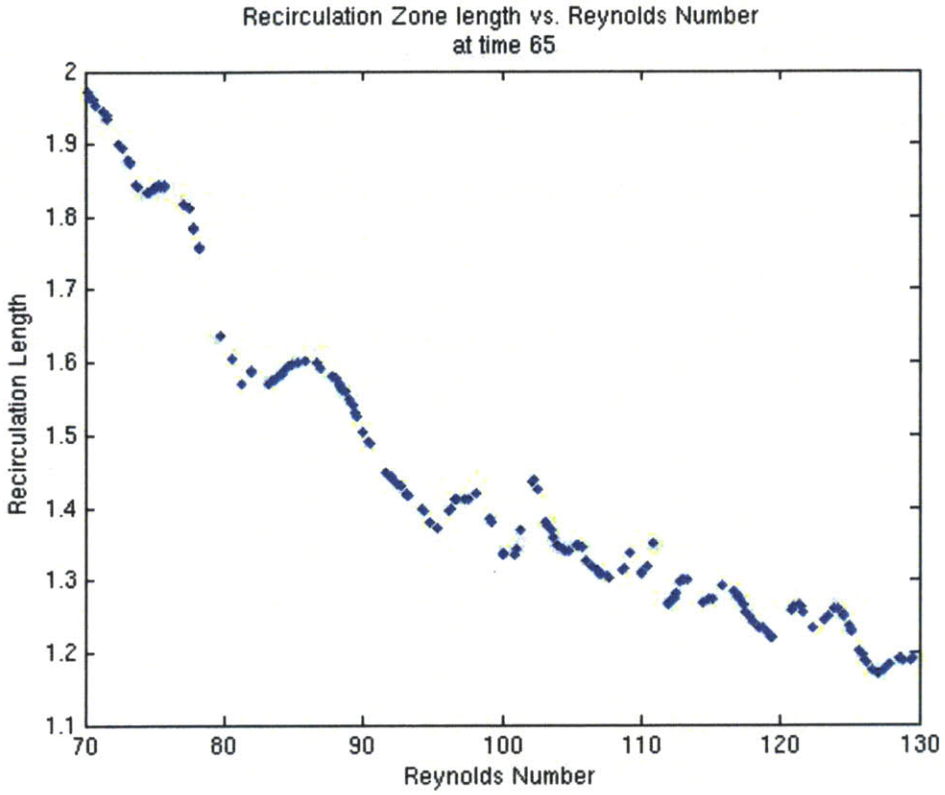

Figure 19: Very High Reynolds Number,
Non-dimensional Recirculation Zone Length (Case 11)

4.2 Vortex Shedding

In addition to estimating the recirculation length and its dependence on the Reynolds number, we can measure the vortex-shedding period for the different stochastic cases that we simulated. As mentioned in the introduction, at larger Reynolds numbers (Re> Re_{crit}) flow separation occurs. When we pass the critical Reynolds number, Re_{crit}, we observe a well-known phenomenon: the von Karman vortex street with periodic vortex motion.

The vortices however, move with time so calculating this frequency is not trivial. Once again, we look to the velocity components on the grid. To measure this oscillatory motion, we can track one spatial point over several time steps instead of many spatial points at one time step as was done for the recirculation zone length calculation. We monitored the vertical velocity component at a single point at the bottom of the cylinder, and a fixed number of units points in to the wake at location $(x, y) = (10,0)$ to allow for sufficient space for eddies to completely mature into full vortices. Next, we observe when the vertical velocity component changes sign from up to down. This gives us the entire period and therefore, allows us to track the shedding frequency.

We also compare these properties for different mean Reynolds numbers. Based on the existing literature, the threshold for the appearance of dynamical characteristics such as the vortex shedding frequency or the recirculation zone length varies with the Reynolds number of the fluid flow. In our simulations, we estimate such characteristic for stochastic flows with mean Reynolds numbers of 20, 40, 60, and 110. For each of these cases, we calculated the shedding period and recirculation length of every the Reynolds number range captured in the DO simulation, and compared results among each other and to those in the literature. In our case, the shedding period is related to the Strouhal number as St = L/UT, where L is the length of the side of the cube, U is our non-dimensional velocity, and T is the shedding period.

For the low Reynolds number case (Figure 20), there was no evidence at all of a vortex shedding period. This shows that our method is correct in this case because within this range, the flow will exclusively exhibit the recirculation zone length behavior. This is

consistent with previous literature which expresses Re_{crit} to be a number less than 70. The lowest value found by Klekar and Patankar (1992) also found a $Re_{crit} = 54$, suggesting that no vortex shedding should occur for the low Re range examined by our first case.

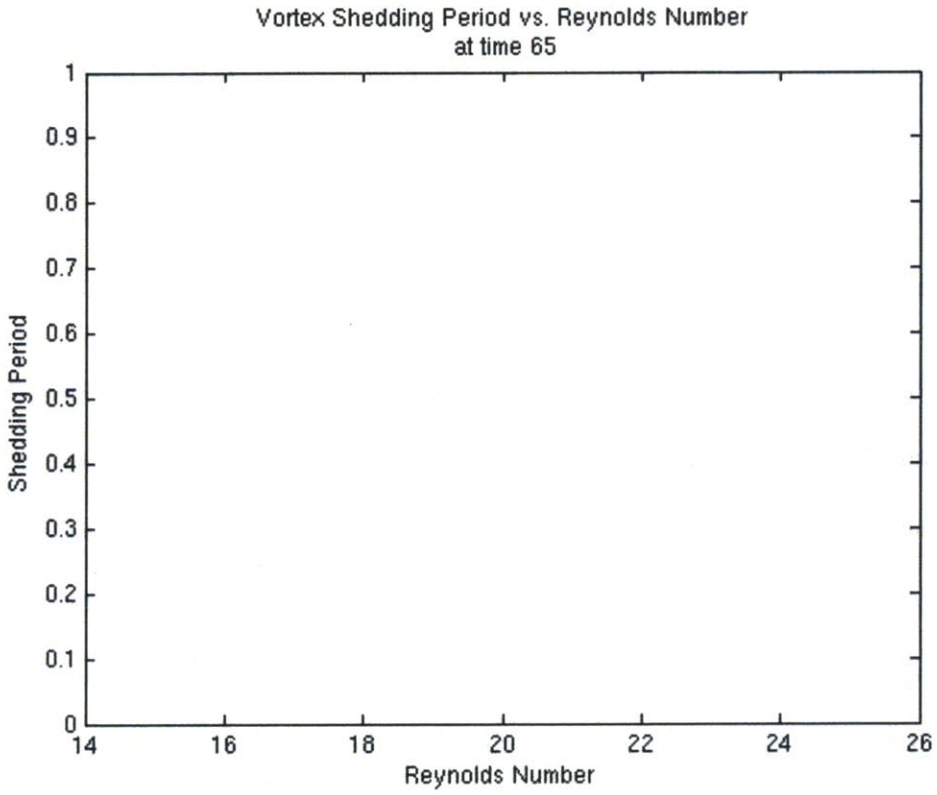

Figure 20: Low Reynolds Number, Non-dimensional Vortex Shedding Period (Case 3)

It is for the Mid Reynolds number case (Figure 21) that we first see evidence of Vortex shedding. Figure 21 illustrates the Vortex shedding period for the different Reynolds number values. There is a clear correlation: the higher the Reynolds number, the smaller the period (or higher the frequency). The estimated slope if we assume it is linear, is -0.01156, with a covariance of 0.0015 and standard deviation of 0.0383. The covariance

and standard deviation values are derived from the average error produced by calculating the slopes over many of the data points used in the fit to a line.

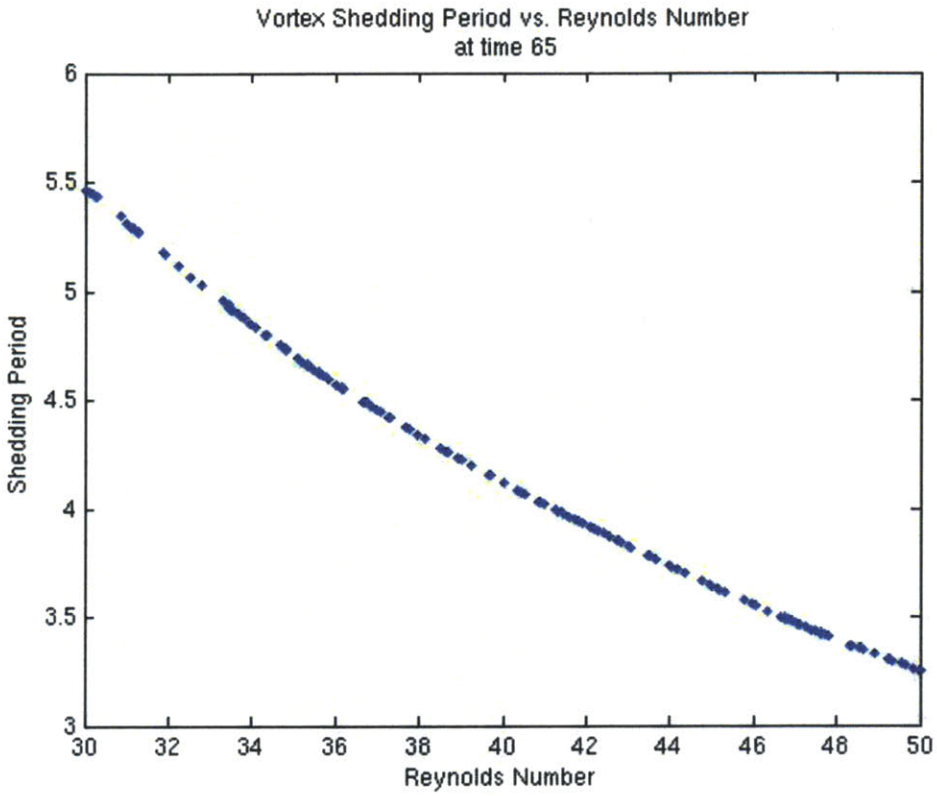

Figure 21: Mid Reynolds Number, Non-dimensional Vortex Shedding Period (Case 2)

For the high Reynolds number cases (Figure 22), the vortex shedding phenomenon becomes much more apparent. Once again, there is a clear correlation: the higher the Reynolds number, the smaller the period (or higher the frequency). The estimated slope, if we assume a linear relation, is -0.0748, with a covariance of 0.0066 and standard deviation of 0.0256. In this model, it is clear that the higher DO modes show there is vortex shedding

as discussed in the previous section. With the downward trend, these results are consistent with the researched findings as well as the governing fluid dynamic equations.

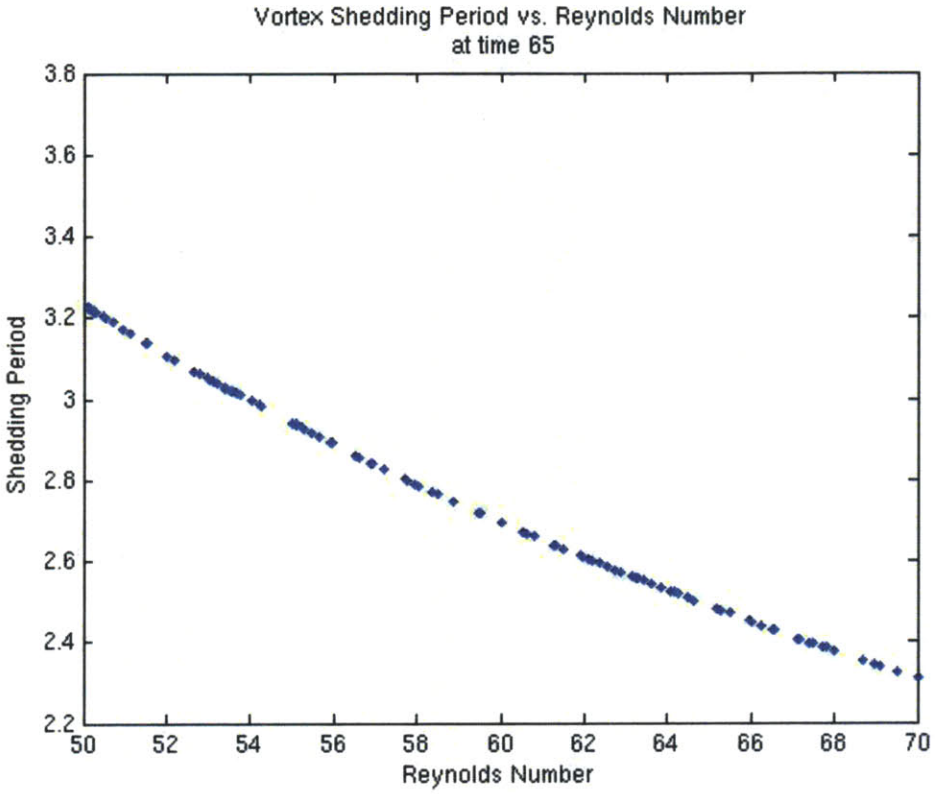

Figure 22: High Reynolds Number, Non-dimensional Vortex Shedding Period (Case 4)

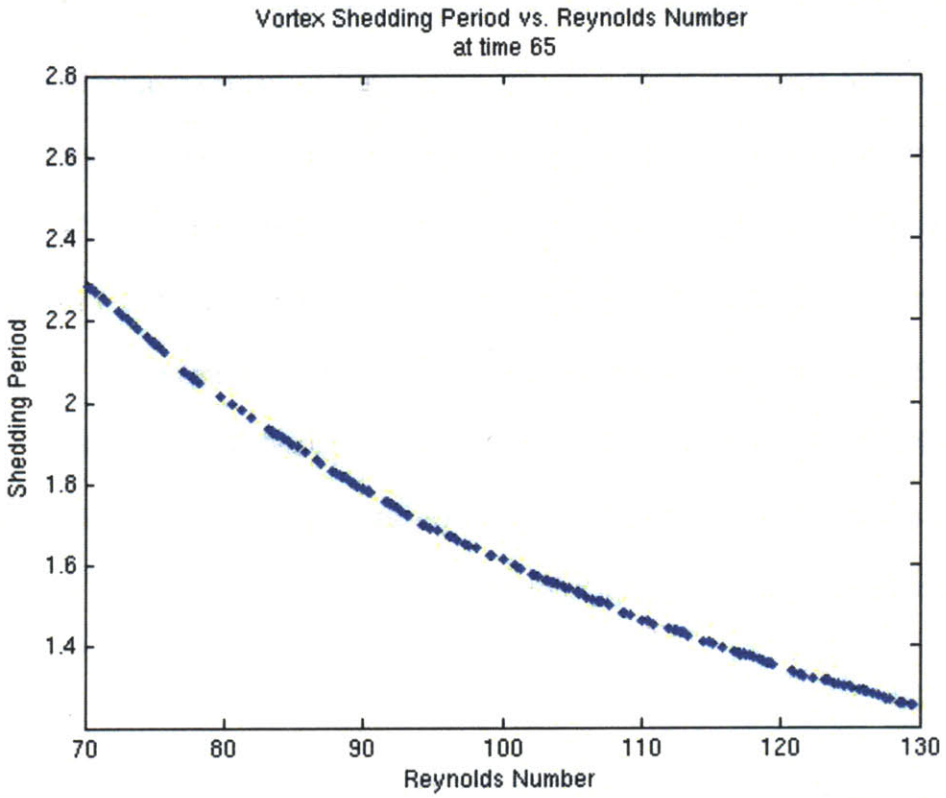

Figure 23: Very High Reynolds Number, Non-dimensional Vortex Shedding Period (Case 11)

For the very high Reynolds number case (

), the results are similar to the previous high Reynolds number case. The slope is still negative, which points to the negative correlation between the Reynolds number and vortex shedding period. However, there is an apparent largest curvature around Re = 90. The relation is clearly not linear for all Re regimes. This is also mentioned in previous literature. For example, Lin et al (2007) found for the circular cylinder case that the shedding frequency from (0.1592, 0.1697) for the Reynolds number range (90, 110). This is equivalent to (6.28, 5.89) in non-dimensional time units or periods. If we non-dimensionalize their results the same way we non-dimensionalized our, we obtain a shedding period of (2.51, 2.36), which is close to our result if we keep in mind that Lin et al (2007) used a circular cylinder and a wider domain.

Vortex Shedding Summary: In the previous literature, Frank (1990) pioneered the comparative study of vortex shedding frequency to lift coefficients and to the size of eddies. As mentioned in section 1.2, there have been many different estimates for when the onset of vortex shedding occurs for the square cylinder case. Kelkar et. al. reported 53, Norgberg estimated 47 with a deviation of 2, Sohankar et al. reported its value to be 51.2 standard deviation of 1.0. Although the hasn't been one solution deem correct since the result depends on fluid characteristics like Prandtl and Strouhal numbers, our DO simulation results fall within this range by displaying characteristics of periodic vortex shedding when the Reynolds number reaches 43.

Table 5: Mean Slopes of Recirculation Zone Length and Vortex Shedding Plots
*This slope comes from only the upward trend in the left sub graph in the Figure with the Recirculation zone length for the base case (

).

		Recirculation Zone Length			Vortex Shedding Period		
Reynolds Number	Cases	Average Slope	Covariance	Standard Deviation	Average Slope	Covariance	Standard Deviation
20	3	0.0537	1.24×10^{-6}	0.0011	N/A	N/A	N/A
40	2	0.0553*	7.62×10^{-5}	0.0087	-0.1156	0.0015	0.0383
60	4	.	.	.	-0.112	0.0009	0.057
100	11	.	.	.	-0.108	0.0006	0.099

5. Conclusion

Franke (1990) states in the introduction that "A trustworthy numerical method should be able to predict the occurrence of periodic vortex shedding by itself." In this thesis, we used the stochastic Navier-Stokes equations to predict the recirculation zone length and vortex shedding period for a large range of Reynolds numbers in a single simulation. Specifically, we evaluated a new computational scheme that uses a novel open boundary condition formulation for Dynamically Orthogonal (DO) stochastic Navier-Stokes equations. This approach allowed us to model a wide range of random inlet boundary conditions with a single DO simulation of low stochastic dimension, reducing computational costs by orders of magnitude.

In this thesis, we reviewed existing literature, examined our simulation results and validated the numerical solution. The convergence was tested and we validated the numerical solution. We then studied the sensitivity of the results to: the resolution of in the stochastic subspace; the resolution in the physical space; and the number of DO modes. Finally, we evaluated and studied how the recirculation length and the vortex shedding period varied with the Reynolds number.

With the ability to model a range of Reynolds number in a single simulation, the DO method also enables us to determine how different flow characteristics are correlated to the different Reynolds numbers. We found that the recirculation zone length increased linearly with Reynolds number, and the slope of this increase was approximately 0.55. This correlation was only valid up until the Reynolds number where the dynamics changed to periodic shedding, or for $Re < 40$. The literature agrees with our findings, suggesting that

this curve should follow a linear slope of 0.0553 (Bruer 1999). Additionally, for Re > 42 we found that the vortex shedding period decreased nearly linearly with increased Re, and this also agreed with existing literature. We obtained shedding periods of [1.8, 1.6] for Reynolds numbers [90, 100]. While we could not find results for the same problem setup, our results compare well with the results of Lin et. al. (2007) who found shedding periods of [2.51, 2.36], for the same Reynolds numbers but using a circular cylinder and a wider domain. Our results fall below this range but it is expected that the vortex shedding period is larger and broader for the square cylinder case.

When the DO method is combined with the new open boundary condition formulation, it is a very efficient alternative to the current stochastic modeling methods available because of its unique approach to decomposing the Navier-Stokers equation with uncertain parameters. This new approach can be used to quantify uncertainty in large fluid dynamic systems, such as weather or ocean predictions. Coupled with new data-assimilation methods that take advantage of the non-Gaussian statistics, the accuracy of numerical ocean and weather prediction can be improved. Additionally, we have shown that this method can be used to determine correlations between flow characteristics and uncertain parameters for a simple case. In the future, this method could be used for more complex problems to determine engineering design parameters. This thesis brings the DO methodology one step closer to practical applications.

Bibliography

Bruer, M., Bernsdorf, J., Zeiser, T., Durst, F. (1999). Accurate computations of the laminar flow past a square cylinder based on two different methods: lattice-Boltzmann and finite-volume. *International Journal of Heat and Fluid Flow*, 21:186-196.

Cameron RH, Martin WT (1947) The orthogonal development of nonlinear functionals in series of Fourier-Hermite functionals. Ann of Math 48:385-392.

Chen D, Liu J (2000) Mixture Kalman lters. J Roy Statist Soc Ser A 62:493-508.

Deb MK, Babuska I, Oden J (2001) Solution of stochastic partial differential equations using Galerkin finite element techniques. Comput Methods Appl Mech Eng 190:6359-6372

Doucet A, de Freitas N, Gordon N (2001) Sequential Monte-Carlo Methods in Practice. Springer-Verlag.

Erturk E, Corke TC, G□bkc□bl C (2005) Numerical Solutions of 2-D Steady Incompressible Driven Cavity Flow at High Reynolds Numbers. *International Journal for Numerical Methods in Fluids* 48:747-774.

Franke, R., Rodi, W., Schöung, B. (1990). Numerical Calculation of Laminar Vortex-shedding Flow past Cylinders. *Journal of Wind Engineering and Industrial Aerodynamics*, 35:237-257.

Galletti, B., Bruneau, C. H., Zannetti, L., and Iollo, A. (2003). Low-order modelling of laminar flow regimes past a confined square cylinder. *Journal of Fluid Mechanics*, 503:161-170.

Haley PJ Jr, Lermusiaux PFJ (2010) Multiscale two-way embedding schemes for free-surface primitive-equations in the Multidisciplinary Simulation, Estimation and Assimilation System (MSEAS). Ocean Dynamics 60:1497-1537.

Kelkar, K. M., Patankar, S. V. (1992). Numerical Prediction of Vortex Shedding Behind a Square Cylinder. *International Journal for Numerical Methods in Fluids*, 14:327-341.

Lermusiaux, P.F.J. (1999). Estimation and study of mesoscale variability in the Strait of Sicily. Dynamics of Atmospheres and Oceans, 29, 255-303.

Lermusiaux PFJ (2006) Uncertainty estimation and prediction for interdisciplinary ocean dynamics. *Journal of Computational Physics*, 217:176-199.

Lin, G., Wan X., Chau-Hsing, S., Karniadakis, G. E. (2007). Stochastic Computational Fluid Mechanics. *Computing in Science and Engineering*. 9(2):21-29.

Robichaux, J., Balachandar, S., and Vanka, S. P., Two-Dimensional Floquet Instability of the Wake of Square Cylinder, Phys. Fluids, vol. 11, pp. 560–578, 1999.

Sapsis TP (2010) Dynamically orthogonal field equations for stochastic fluid flows and particle dynamics. Ph.D Thesis, Massachusetts Institute of Technology, Department of Mechanical Engineering.

Sapsis TP, Lermusiaux PFJ (2009) Dynamically orthogonal field equations for continuous stochastic dynamical systems. Physica D 238:2347-2360.

Sen, S., Mittal, S., Biswas, G. (2010). Flow past a square cylinder at low Reynolds numbers. *International Journal for Numerical Methods in Fluids*. 67:1160-1174.

Sharma, A., Eswaran, V. (2004). Heat and Fluid Flow Across a Square Cylinder in the Two-Dimensional Laminar Flow Regime. *Numerical Heat Transfer, Part A: Applications*. 45(3): 247-269.

Sohankar, A., Davidson, L., and Norberg, C. Numerical Simulation of Unsteady Flow around a Square Two-Dimensional Cylinder, Proc. 12th Australian Fluid Mechanics Conf., Sydney, Australia, pp. 517–520, 1995.

Sohankar, A., Norberg, C., and Davidson, L. Numerical Simulation of Unsteady Low-Reynolds Number Flow around Rectangular Cylinders at Incidence, J. Wind Eng. Ind. Aerodyn., vol. 69, pp. 189–201, 1997.

Ueckermann, M. P., Lermusiaux, P. F. J., Sapsis, T.P. (2012). Numerical Schemes for Dynamically Orthogonal Equations of Stochastic Fluid and Ocean Flows. *Journal for Computational Physics*.

Van Dyke, M. *An Album of Fluid Motion*, The Parabolic Press, Stanford, 2002. (image)

Venturi, D., Wan, X., Karniadakis, G. E. (2008). Stochastic low-dimensional modeling of random laminar wake past a circular cylinder. *Journal of Fluid Mechanics*. 606:339-367.

Xiu D (2010) Numerical Methods for Stochastic Computations: A Spectral Method Approach. Princeton University Press.